h

SANDIA REPORT

SAND2004-6445
Unlimited Release
Printed December 2004

Next Generation Spindles for Micromilling

D. D. Gill, B. Jokiel Jr., J. C. Ziegert, S. W. T. Payne, and J. P. Pathak

Prepared by
Sandia National Laboratories
Albuquerque, New Mexico 87185 and Livermore, California 94550

Sandia is a multiprogram laboratory operated by Sandia Corporation,
a Lockheed Martin Company, for the United States Department of Energy's
National Nuclear Security Administration under Contract DE-AC04-94AL85000.

Issued by Sandia National Laboratories, operated for the United States Department of Energy by Sandia Corporation.

Available to DOE and DOE contractors from
U.S. Department of Energy
Office of Scientific and Technical Information
P.O. Box 62
Oak Ridge, TN 37831

Telephone: (865)576-8401
Facsimile: (865)576-5728
E-Mail: reports@adonis.osti.gov
Online ordering: http://www.osti.gov/bridge

Available to the public from
U.S. Department of Commerce
National Technical Information Service
5285 Port Royal Rd
Springfield, VA 22161

Telephone: (800)553-6847
Facsimile: (703)605-6900
E-Mail: orders@ntis.fedworld.gov
Online order: http://www.ntis.gov/help/ordermethods.asp?loc=7-4-0#online

SAND 2004-6445
Unlimited Release
Printed December 2004

Next Generation Spindles for Micromilling

David D. Gill
Manufacturing Engineering and Process Development Department

Bernhard Jokiel Jr.
Advanced Packaging Department

Sandia National Laboratories
P.O. Box 5800
Albuquerque, NM 87185-0958

John C. Ziegert, Scott W. T. Payne, and Jay P. Pathak
Machine Tool Research Center
Department of Mechanical and Aerospace Engineering
University of Florida
Gainesville, FL 32511

Abstract

There exists a wide variety of important applications for micro- and meso-scale mechanical systems in the commercial and defense sectors, which require high-strength materials and complex geometries that cannot be produced using current MEMS fabrication technologies. Micromilling has great potential to fill this void in MEMS technology by adding the capability of free form machining of complex 3D shapes from a wide variety and combination of traditional, well-understood engineering alloys, glasses and ceramics. Inefficiencies in micromilling result from the relationships between a cutting tool's breaking strength, the applied cutting force, and the metal removal rate. Because machining times in mesofeatures scale inversely to the part size, a feature $1/10^{th}$ as large will take 10 times as long to machine. Also, required chip sizes of 1 m or less are cut with tools having edge radius of 2-3 m, the cutting edge effectively has a highly negative rake angle, cutting forces are increased significantly causing chip loads to be further reduced and the machining takes even longer than predicted above. However, cutting forces do not increase with cutting speed, so faster spindles with reduced tool runout are the path to achieve efficient mesoscale milling.

This research explored the development of new ultra-high speed micromilling spindles. A novel air-bearing spindle design is discussed that will run at very high speeds (450,000 rpm) and provide very minimal runout allowing the best use of micromilling cutters and reducing overall

machining time drastically. Two generations of this spindle design were completed; one with an air bearing supported tool shaft and one with a novel rolling element bearing supported tool shaft. Both designs utilized friction-drive systems that relied on diameter differences between the drive wheel (operating at speeds up to 90,000 rpm) and the tool shaft to achieve high rotational tool speeds. Runout, stiffness, and machining tests were conducted with the spindle designs and though they both showed promise for ultra-high speed machining, runout issues in the friction drive and in the stock tools kept the system from achieving sustained machining capability.

Contents

Figures

Tables

Next Generation Spindles for Micromilling

David Gill, Bernhard Jokiel Jr., John Ziegert, Scott Payne, Jay Pathak

Introduction

Micromachining is an emerging fabrication technology that broadens applicable material ranges including metals and plastics. It is also envisaged as the technology of choice to create complex three-dimensional shapes in hard engineering materials. It could lead to the rapid and direct manufacturing of micro-molds and masks to aid in development of micro-components. The micromilling process is characterized by milling tools that are currently in the range of 22-100 μm. These tools are inexpensive and widely available. Currently, these tools are used to create miniature features in plastics, graphite, and some soft metals. They are characterized by a relatively low material removal rate (MRR), which leads to longer process times. In order to reduce the process time, much higher spindle speeds are needed. Commercial high speed spindles can typically reach 100,000 rpm with a few highly specialized spindles reaching 200,000 rpm. To achieve the desired cutting speed in a material, spindle speeds in excess of 500,000 rpm are needed.

Commercially available micromilling tools typically have a cutting edge radius on the order of 2 to 3 m. In micromilling, to avoid tool breakage the chip thickness is typically less than 1 m, so the tool edge effectively has a large negative rake angle. This poor cutting geometry increases the effective cutting stiffness, K_s, resulting in even higher forces, and thus requiring an even smaller chip thickness, further slowing the feed rate and increasing the processing time.

Typical milling spindles used for these small tools employ either rolling element bearings or air bearings to support the spindle shaft. Tools are typically clamped in such spindles using a collet or set screw. The combination of asynchronous spindle bearing error motions and clamping errors often result in tool runout 3 to 20 times the nominal chip thickness. This will drastically increase the cutting force and may lead to tool breakage unless the axial depth of cut is reduced, thus further reducing the MRR and increasing the processing time. As a result, the tool spends most of its time under-loaded to protect against the few times when the spindle and clamping errors cause excessively thick chips to be cut.

The goal of this research is the creation of a spindle that greatly reduces the combined causes of tool runout and at the same time greatly increases the rotational speed of the spindle, thus yielding increased tool life and significantly improved material removal rates

Literature Review

A review of the literature regarding micromilling has identified several characteristics of micromilling which significantly distinguish it from conventional milling. These include:

Cutting Forces. Because of the small diameter of the tools, the cutting forces must be kept very small so as not to exceed the bending stress fatigue limit of the tool at the root. In calculation of cutting forces, several models are proposed in different papers. Tansel's [1] analytical cutting force sounds very convincing as it considers the chip thickness by considering the trajectory of the tool tip while the tool rotates and moves ahead continuously. Tlusty's [2] cutting force model which considers the tool tip path as circular arcs that are mutually shifted by f_t (feed per tooth) is no longer valid for micromilling as the ratio of feed per tooth and tool radius is *not* very small. Tansel's model takes care of this issue.

Chip Load: In order to keep the forces sufficiently small, the chip thickness must be very small. Typical values reported for machining of metallic workpieces are on the order of 0.5 to 1.0 micrometers.

Cutting Edge Radius: Commercially available micro-end mills typically have cutting edge radii on the order of 2 to 3 micrometers, or 2 to 6 times the chip thickness. This means that the effective rake angle of the cutting edge is highly negative, on the order of –45 to –60 degrees. In this situation, the conventional models of the mechanics of chip formation do not apply, and the cutting force coefficients are typically 20 to 40 times higher than in conventional milling.

Spindle Runout: The problem of small chip thickness is complicated by the fact that typical milling spindles have radial runout at the tool tip on the order of 1 to 2 micrometers or more [3] [4]. This means that in ordinary operation, some teeth on the cutter may not contact the workpiece at all during rotation, while others are forced to cut chips up to several times the desired thickness. This leads to overloads of the tool and premature failure.

Cutting Speed: Spindle speeds are normally chosen in order to make the tangential velocity of the cutting edge through the workpiece high enough to achieve efficient cutting. For instance, when using carbide tools to machine aluminum, the recommended cutting speed is on the order of 500 meters/minute. To achieve this cutting speed with a tool diameter of 0.25 mm, the required spindle speed is over 600,000 rpm. This speed is unachievable with current machine tool spindle technology.

Feed rate: With a 1 micrometer chip thickness and a 2 fluted cutter, the feed rate is only 2 micrometers per revolution. Therefore, if the spindle speed is 20,000 rpm (a typical maximum spindle speed for a high speed milling spindle), the feed rate of the tool through the work is only 40 mm/min. This results in very low material removal rates and excessively long machining times.

Tool wear: Unpredictable tool life and premature tool failure are the major concerns in micro machining using micro grain carbide cutters. The helix angle plays an important role on tool life [6]. Bao and Tansel [7], [8] modified their analytical model [1] to represent tool wear.

In addition to these issues papers were reviewed on the application of micromilling to different materials including cast iron [5], copper [6], and aluminum [8]. A high precision mciromilling spindle design is presented in [9], which addresses the problems of runout.

Summary of Findings

Based on the literature review, it is apparent that inadequacies in micromilling spindle technology are currently a limiting factor for this technology. To illustrate, consider a given part geometry that is to homogenously scale down in size by a scaling factor, ***k,*** where $k < 1$. The cutting tools are also scaled by the same factor. If the spindle speed is constant for both operations, the feed rate must scale by a factor of k^2 to maintain a constant bending stress in the tool, while the axial and radial depths of cut each scale by the factor, ***k***. Therefore, the MRR scales by k^4, while the volume of material to be removed scales by k^3. This means that if a certain mechanical component is to be created by an end milling operation and a geometrically similar component one-tenth the size is also to be created, the operation will take approximately ten times as long to complete. In order to avoid this, the spindle speed must increase by a factor of ***1/k***, while maintaining minimal radial runout.

To facilitate the design of the micromilling spindle, values for cutting force, torque, and power needed to run a spindle at speeds up to 500,000 RPM were calculated. A variety of workpiece materials were considered as well as tool diameters ranging from 1/8'' to 1/64'', and spindle speeds ranging from 15,000 rpm to 500,000 rpm. Equation 1 presents the method by which the data presented in Table 1 was calculated utilizing Tansel's Cutting Force Model [1] and a tool bending stress equation presented by Boresi [10].

Tansel's Cutting Force Model:

$$F_x = F_u\left[C_1\frac{f_t}{r}\sin^3\theta + C_2\frac{f_t}{r}\cos^3\theta - \sin^2\theta + \frac{1}{2}p\sin 2\theta - \frac{f_t}{r}\sin\theta - p\theta\right]\Bigg|_{\theta_s}^{\theta_e}$$

$$F_y = F_u\left[C_2\frac{f_t}{r}\sin^3\theta - C_1\frac{f_t}{r}\cos^3\theta - p\sin^2\theta - \frac{1}{2}\sin 2\theta - p\frac{f_t}{r}\sin\theta + \theta\right]\Bigg|_{\theta_s}^{\theta_e}$$

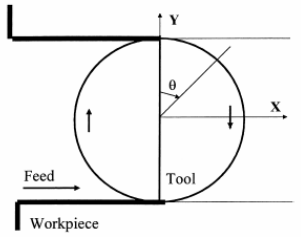

Model co-ordinate system for end milling operation.

Where, $C_1 = \frac{1}{3}\left(1 + p\frac{Z}{\pi}\right)$, $C_2 = \frac{1}{3}\left(p - \frac{Z}{\pi}\right)$, $F_u = \frac{K_m r f_t}{2\tan\beta}$

Also,

- Fx: Cutting force in feed direction.
- Fy: Cutting force in normal direction.
- Fu: Unit force.
- Km: Material coefficient.
- Z: No. of teeth.
- p: Ratio of Fn/Fc.

Table 1. Cutting Force, Required Torque, and Power Calculated for Several Spindle Speeds

Dia (m)	Speed (rpm)	Feed (mpm)	Feed /tooth (m)	W of cut (µm)	D of cut (µm)	Fx (N)	Fy (N)	Torque (N-m)	Power (W)
5.08e-4	500,000	2.54e-1	2.54e-7	508	254	1.66	2.86	8.43e-4	4.41

5.08e-4	700,000	5.08e-1	3.63e-7	508	254	2.37	4.09	1.2e-3	8.83
5.08e-4	600,000	2.54e-1	2.12e-7	508	254	1.38	2.38	7.03e-4	4.41
5.08e-4	600,000	3.81e-1	3.18e-7	508	254	2.08	3.58	1.05e-3	6.62

Ultra-High Speed Spindle Design – Generation 1

In light of the fact that there are no spindles available which can run at speeds even approaching 500,000+ RPM, innovative concepts are needed for achieving these spindle speeds. This research utilizes the tool shank itself as the spindle shaft and uses a friction drive with drive ratio of 9:1 to transmit the torque from a commercially available high speed (90,000 rpm) spindle, as shown in Figure 1. Commercially available micromilling cutters typically have a 0.125-inch diameter shank, approximately 1.5 inches long. The cutting edges of the milling cutter are ground into the end of the tool shank. Instead of clamping the tool shank into the rotating shaft and collet of the spindle, the spindle design supports the tool shank radially and axially in a porous carbon air bearing. The tool shank effectively becomes the "spindle shaft" which decouples spindle and collet errors from the tool. This reduces the error motion of the tool to only runout in the tool which is routinely kept to the sub-micrometer level in these tools.

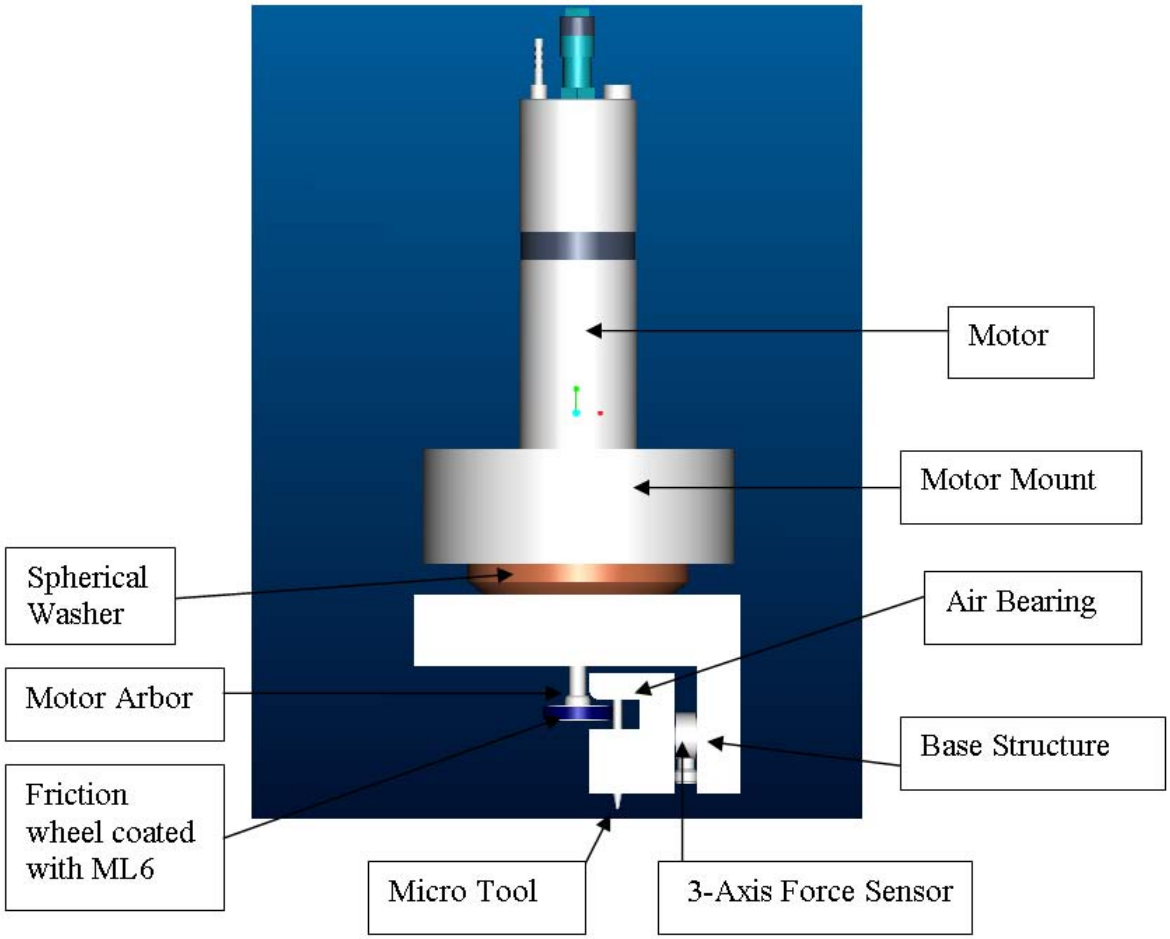

Figure 1. Illustration of Ultra High Speed Spindle

Description of the Design

The micromilling spindle system consists of the following components:

- A customized air-bearing capable of using 1/8'' diameter shank microtools.
- A 3-axis force sensor for the measurement of in-situ milling forces.
- A high speed spindle which can transmit a torque of 0.01 N-m at 50,000 rpm.
- A computer interface to control and display spindle speed, monitor tool forces during milling and provide means to interpret and feedback milling forces to identify tool breakage and identify and control tool over/under-loading.

The air bearing used to support the tool shaft was custom manufactured for this application by New Way Machine Components, Inc. Figure 2 shows a solid model of the bearing with the bearing surface in red and the aluminum housing in grey. The horizontal slot on the front face of the housing is the access for the friction drive wheel to drive the tool shaft. Figure 3 shows the air bearing as mounted in the spindle assembly with the drive wheel positioned in contact with the tool shaft. For the air bearings to work properly the manufacturer recommended a shaft tolerance of +/-0.00015 inches. However, the commercially available micro-tools have a shaft tolerance of +/-0.0005 inches. Therefore, a collection of micro-tools was purchased and the shaft diameters measured. The air bearing bore was sized to fit these tools. The micro-tools float freely inside the air-bearing when it is supplied with air, indicating that the bearing was sized appropriately, but the lack of tolerance control would be an important consideration for widespread use of this design. In fact, when later tools that satisfied the diameter requirements were causing wear in the air bearing, a set of measurements was taken to determine the cylindricity of the tool shafts. Again, it was found that while many of the tools had fairly low cylindricity, a few tool shafts were of significantly different tolerancing. The measurements for 8 randomly sampled tool shafts is shown in Table 2 where it can be seen that two shafts have significantly higher cylindricity values than the other six tools. This highlights the need to have more precisely produced tools or to do 100% inspection on tools meant to be used in high precision bearings.

The bearing itself is supported on 3-axis force sensor (Kistler 9017A) to measure the cutting forces in 3 perpendicular directions with a resolution of 0.01N and a measuring range of +/-1kN. The force measurements allow the operator or control system to sense the total force on the tool, which was to be used to sense when the tool touches the part surface for tool setting and for monitoring of the cutting forces during operation to sense tool breakage and wear. It was also intended to be used to modulate the feed rate to avoid overloading or under-loading the tool.

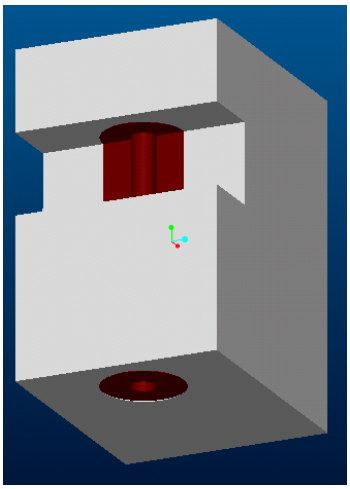

Figure 2. Solid Model of Air Bearing Showing Porous Carbon Bearing in Red and Aluminum Housing in Gray

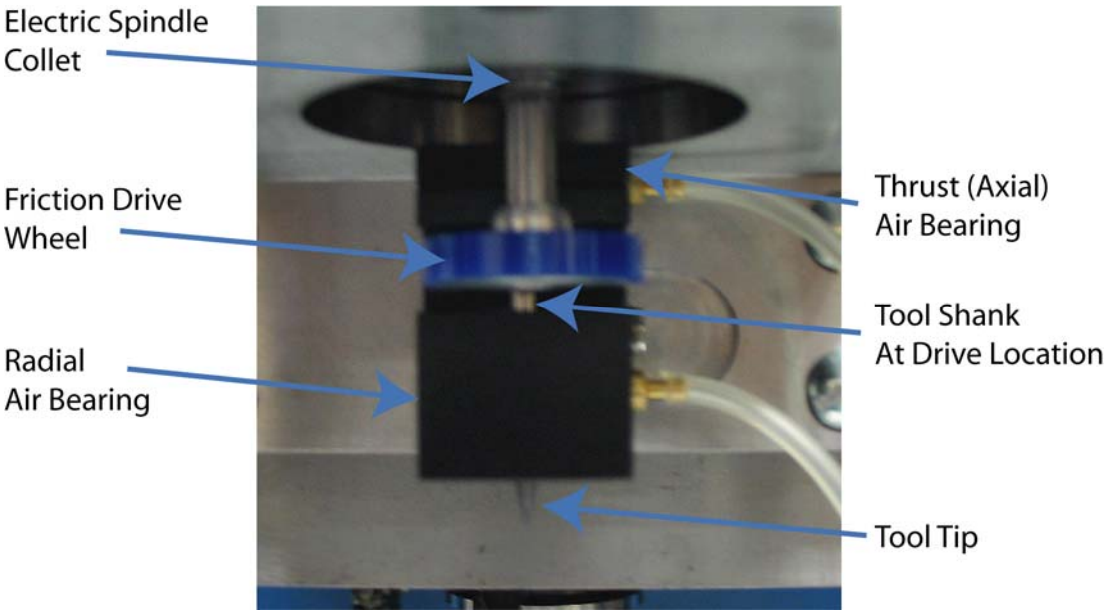

Figure 3. Friction Wheel Drives Tool Shank Supported Axially and Radially in Air Bearing

A 1 inch diameter friction wheel, shown in Figure 4 drives the 0.125-inch tool shank. The friction wheel, clamped firmly in the drive spindle's collet, is driven by a commercially available AC asynchronous, induction motor (Precise Corp. SC 40 Spindle), which develops a rated 0.21 KW of power at 90,000 RPM. With the drive spindle rotating at this speed, the difference in radius between the drive wheel and the tool shaft causes the tool to rotate at speeds as high as 700,000 RPM. A thin layer of compliant high friction material (ML-6 from Meridian Laboratory) is coated on the friction wheel to isolate the error motions of the motor, spindle, and collet from the tool shaft and to prevent slip at the interface between the drive wheel and the tool shaft.

Table 2. Cylindricity Measurements from 8 Tool Shafts with 240 Measurement Points at Three Elevations Per Shaft

Tool Number	1	2	3	4	5	6	7	8
Top Dia (in)	0.12476	0.12473	0.1247	0.12475	0.12479	0.12459	0.12465	0.12469
Top Circularity (in)	0.00011	0.00014	0.00014	0.00016	0.00013	0.00014	0.00014	0.00013
Center Dia (in)	0.12487	0.12481	0.12482	0.12477	0.12486	0.12468	0.12477	0.12474
Center Circularity (in)	0.00011	0.0001	0.00013	0.00011	0.00013	0.00011	0.00013	0.00011
Bottom Dia (in)	0.12489	0.12481	0.12482	0.12483	0.12488	0.12473	0.12479	0.12474
Bottom Circularity (in)	0.00011	0.00011	0.00013	0.00013	0.00012	0.00011	0.00010	0.00011
Cylindricity (in)	0.00132	0.0004	0.00018	0.00018	0.00019	0.00022	0.00122	0.00018
Cyl. Std Dev. (in)	0.00023	0.00007	0.00003	0.00003	0.00003	0.00004	0.00027	0.00003
Number of points	2751	2766	2749	2758	2747	2756	2768	2769
Cylindricity (um)	**33.528**	**10.16**	**4.572**	**4.572**	**4.826**	**5.588**	**30.988**	**4.572**

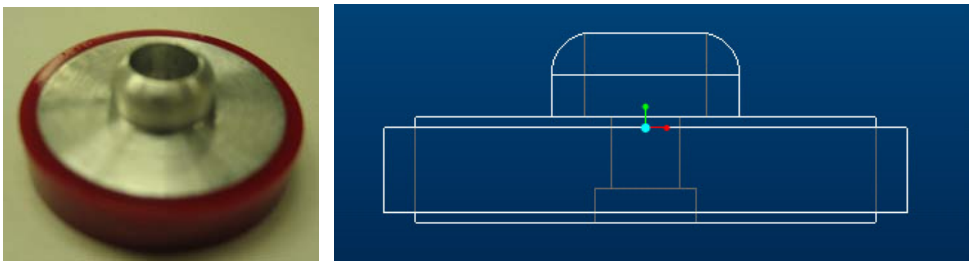

Figure 4. Friction Wheel (Left) Coated with ML-6 (Red) Compliant Friction Coating and Drawing of the Wheel (Right)

The drive spindle motor is mounted on the base structure with a spherical washer set and 4 fine (80 threads per inch) pitch adjusting screws. This arrangement allows the motor axis to be tilted in two perpendicular directions to obtain the necessary normal force on the periphery of the tool shank to maintain high frictional force in order to avoid any slip that might occur. The adjustment also allows the axis of the friction wheel to be slightly tilted relative to the tool shank axis, so that the friction force has a small vertical component, forcing the tool shank vertically against the thrust air-bearing.

A control system was created for the spindle using a National instruments NI DAQ -1200 card which features digital triggering capability; three 16-bit, 8 MHz counters/timers; two 12 bit analog output channels; 24 digital I/O lines and four12 bit differential analog input channels. Three of the input channels are used for force measurements in x, y and z direction. One output channel is used to provide a variable DC voltage from zero to ten volts to command the Precise Motor to rotate from 0 to 90,000 rpm. The two frequency counters are used for measuring the actual speed of the Precise Motor. Five of the digital lines of port A are used for creating virtual LEDs in LabView VI (virtual instrument) for various warnings as recommended in the Precise spindle's frequency converter's instruction manual. A breadboard circuit is used for all electrical connections. It consists of a 7404 inverter chip, which is a hardware aid for measuring the frequency of rotation of the Precise motor. There are five registers of 100k ohms each for electrical tuning of the circuit designed for setting the warning signals during the operation of the motor. The LabView VI created for this research monitors and displays all of the sensor data in

a graphical user interface (GUI). This interface, shown in Figure 5, controls the speed of the spindle, displays the actual speed, and has warning LED's for problems such as low spindle speed, large load changes, overloading, etc.

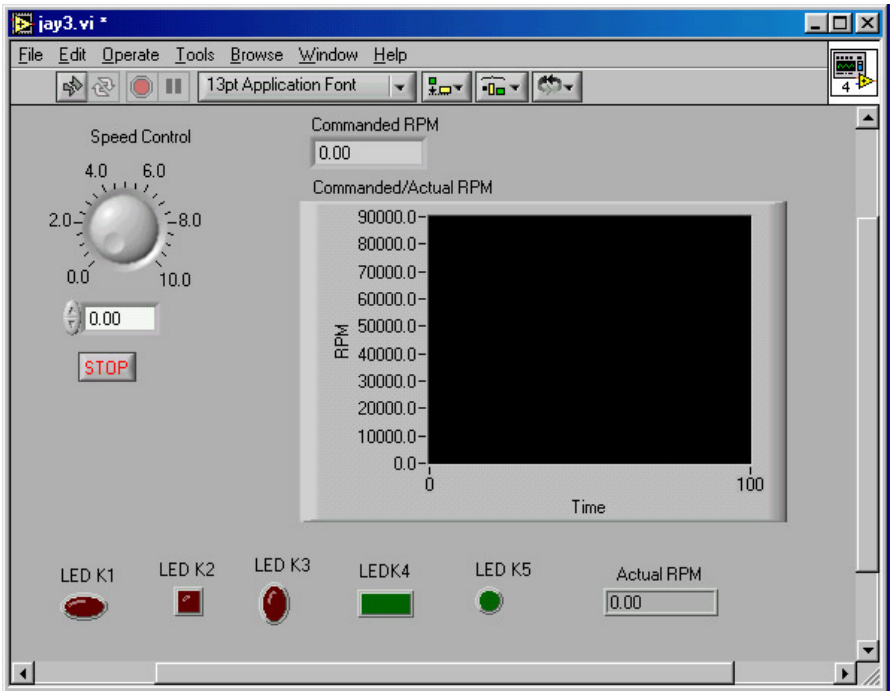

Figure 5. LabView Interface Created for Spindle Control

An additional LabView interface VI was created to monitor the output of the 3-axis force transducer mounted between the air bearing and the spindle assembly mounting block. This interface, shown in Figure 6, was designed to display the X and Y forces, which can be transformed into cutting forces, and the Z force which shows axial thrust.

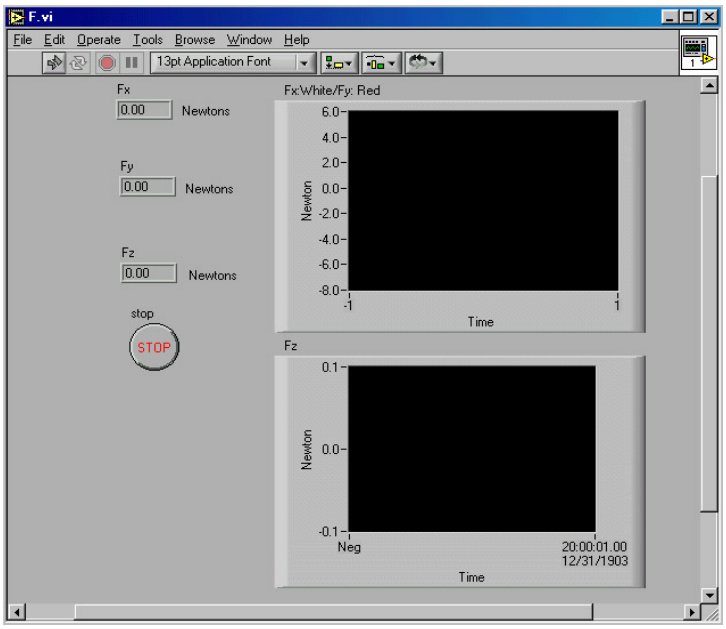

Figure 6. LabView Interface to Display Force Measurement from 3-Axis Load Cell

Design Validation

A finite element analysis (FEA) of the spindle assembly was conducted using the model shown in Figure 7 to predict the first natural frequency of the system. The model represents a tool shaft (middle of the figure) in an air bearing (11 parallel springs at the bottom of figure) being driven by the compliant material on the friction wheel (two springs at the top of the figure). The analysis showed the first natural frequency to be 17,777 Hz when utilizing an aluminum friction wheel. This analysis predicted safe operation of the system up to 12.5 kHz. This analysis translates to a first natural frequency of 85,000 rpm when using an aluminum friction wheel (75,000 rpm with steel) and a safe operating speed of 50,000-75,000 rpm (with an aluminum friction wheel).

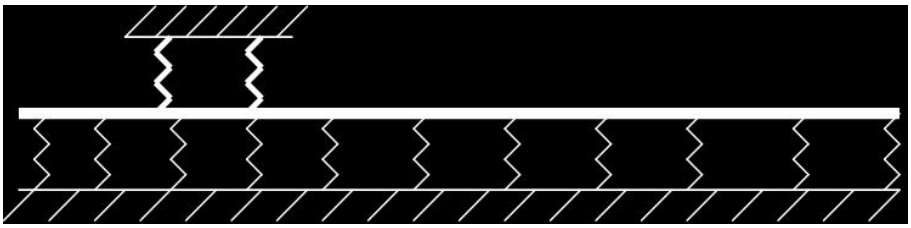

Figure 7. Finite Element Analysis Model Used to Determine the Spindle Design's First Natural Frequency

For this analysis, the projected stiffness of the air bearing was assumed as 42,610 N/m. This value turned out to be difficult to ascertain as there seems to be little means of accurately predicting the stiffness of an oddly shaped air bearing of this size scale before it is constructed. The stiffness depends on the air pressure and on the air gap in the bearing. However, in bearings of this size, the air pressure causes significant deflection in the bearing and an inconsistent air gap. Additionally, very high speed bearings such as this one experience speed related changes in stiffness due to viscosity and temperature effects, both of which are very difficult to predict with

accuracy. It is also very difficult to measure the stiffness in cases other than static testing of the spindle. The *Testing and Analysis of Spindle - Generation 1* details some efforts to attempt to measure this value experimentally.

The analysis also predicted the Hertzian contact stiffness between the friction wheel and tool shaft to be $3x10^8$ N/m. This analysis required an assumption for the modulus of elasticity for the friction coating on the friction wheel. This information was not available from the manufacturer, so a value for urethane was used as this coating is a urethane derivative. The hoop stress in the aluminum friction wheel rotating at 75k rpm was calculated as 34.5 MPa which is well below 76 MPa tensile strength of aluminum. The radial strain in the aluminum friction wheel rotating at 75k rpm was predicted to be 2µm, still within the compliance of the friction material.

Testing and Analysis of Spindle - Generation 1

The testing of the ultra high speed spindle included static testing of the air bearing stiffness and dynamic testing of runout at different locations along the spindle in addition to limited machining tests.

Static Testing of Air Bearing Stiffness

The stiffness of the air bearing needed to be confirmed because the value used in the design was extrapolated from manufacturer's data for larger air bearings. To measure the stiffness, a capacitance gage was used at the end of the spindle, measuring the displacement of the friction wheel. The 3 axis force transducer on the air bearing was used to measure a varying load applied to the wheel while the capacitance probe measured the displacement in real-time. This experiment was repeated several times and typical results are shown in Figure 8 with the resulting stiffness having a value of approximately $5x10^5$ N/m. A second set of measurements was taken with the air pressure turned off in the bearing to check the source of the displacement. These measurements showed the stiffness of the air bearing mounted on the force transducer as being 1 order of magnitude higher than the previously measured stiffness, showing that the displacement of the pressurized measurement was primarily of the shaft in the air bearing.

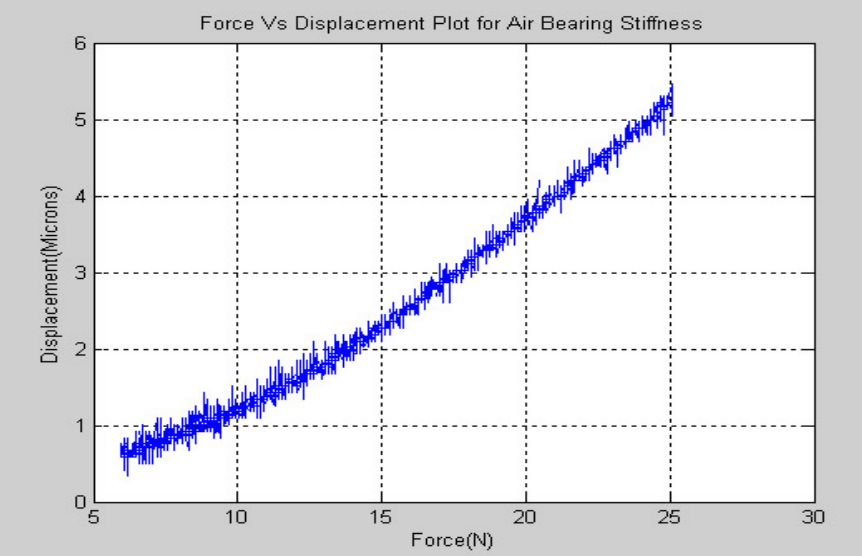

Figure 8. Static Stiffness Plot for the Generation 1 Air Bearing

An alternative method of testing the stiffness was attempted using an instrumented hammer and modal testing techniques. It was determined to be too difficult to precisely strike the very small tool with the relatively large hammer. Another attempt at modal analysis was attempted using a shaker producing swept sine excitation. Again, the large shaker and force transducer made effects of the small mass measuring tool difficult to extract. Further work was done to determine an inverse kinematic model for the system, but an acceptable model that accurately describes the system was never achieved. Figure 9 shows a graph displaying the receptance of the modeled system exhibiting the same trends as the actual data, but with fairly significant differences. Further work in this area was curtailed due to damage to the bearing described later in this document.

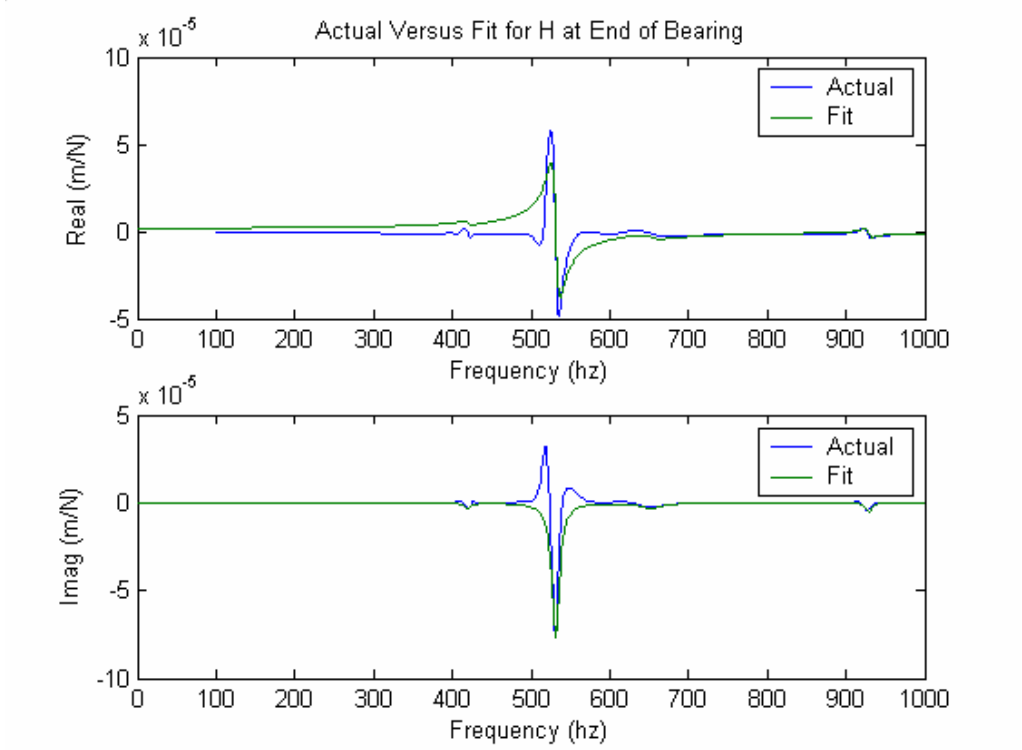

Figure 9. Actual vs. Modeled Receptance as Produced by a Shaker-Induced Swept Sine Wave

Dynamic Testing of Runout

The first dynamic radial runout test was conducted using a capacitance probe mounted to measure the runout of a point along the drive spindle axis. This measurement was made with no tool in the air bearing, but in two configurations, with and without the friction wheel. The results of these measurements are shown in Figure 10 and show the parabolic increase in runout with speed of the drive spindle when the friction wheel is mounted. This shows an imbalance in the friction wheel, either do to eccentricity of the wheel mounting, or an uneven layer thickness in the ML-6 friction coating.

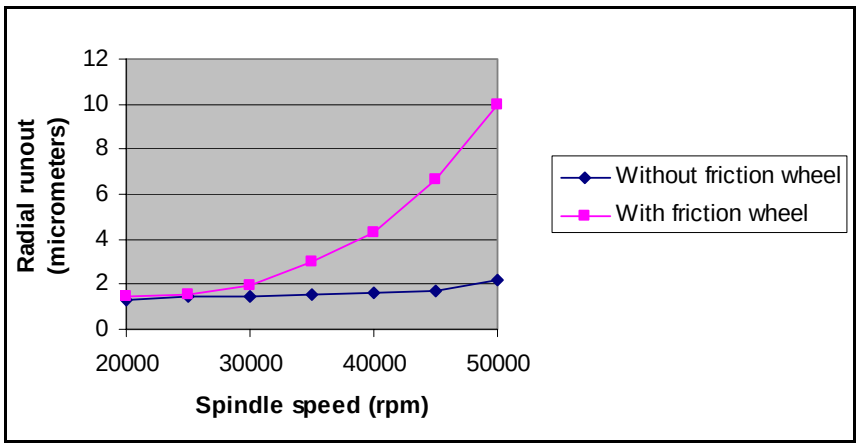

Figure 10. Radial Runout of the Spindle Arbor Measured With and Without the Friction Wheel

Further dynamic measurements compared the runout at the friction wheel to that measured at the end of a gage pin inserted in the air bearing in the place of a tool. The measurements of the friction wheel are made through the friction coating material and thus include effects of the coating thickness as well as the wheel rotational error. These measurements, shown in Figure 11, show the irregularities in the friction wheel to be significant. And, while the compliant friction wheel coating is able to absorb some of the deflections of the friction wheel, it is by no means able to remove all of the noise introduced by the drive spindle, collet, and friction wheel from the tool tip. This spindle design depended on the isolation of the tool from the drive spindle assembly through a very stiff air bearing supporting a tool driven through a low stiffness friction material.

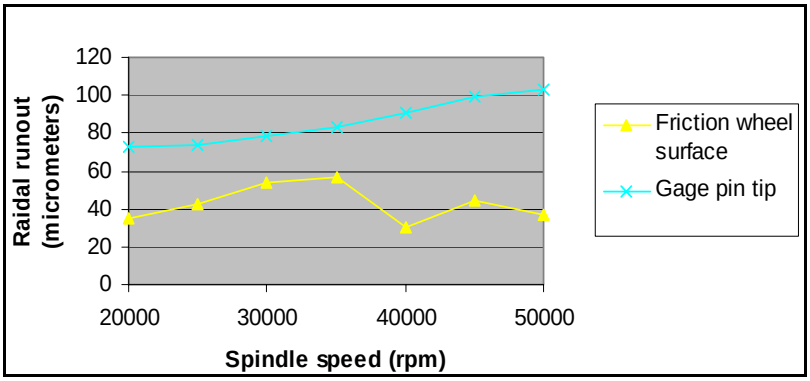

Figure 11. Radial Runout as Measured at the Friction Wheel Surface and at the Gage Pin Tip

Machining Tests and Cutting Force Measurements – Generation 1

The spindle was functionally tested by performing some cutting tests in aluminum. The first set of tests involved creating a set of slots of depths equal to 1/6th and 1/3rd the diameter of the tool with tool diameters from 127-762µm. The tests were run with the spindle operating at a relatively low 79,000 rpm due to the excessive runout in the tool. Measurements of the slots using a measuring microscope showed a significant variation in the slotted depths. For each tool diameter, depth, and width of cut, the feed rate was increased until the tool failed. As an example, Figure 12 shows the feed direction force record for 127µm cutter with a 42.33µm slot depth and the largest achievable feed rate without tool breakage of 0.045 mm/min (0.376 m/tooth). The passage of individual teeth is clearly evident in the force record, and shows that the actual tool speed is approximately 67568 rpm, indicating significant slippage in the friction drive. Significant variation in the peak cutting force is also evident, and may be due to asynchronous error motions of the tool. The cutting force coefficient for these tests was much higher than that predicted by any of the models for macro tools. Figure 13 shows one of the slot cutting experiments for a 508µm tool in aluminum.

A secondary cutting test was performed to determine the minimum wall thickness that could be achieved using hexagonal cutting patterns. These tests showed a minimum wall thickness of 30µm, but the limiting factor was the repeatability of the machine tool, not due to the spindle. These tests, as shown in Figure 14, were to be repeated on Sandia's high precision Moore 350FG, but damage to the air bearing prevented this from occurring.

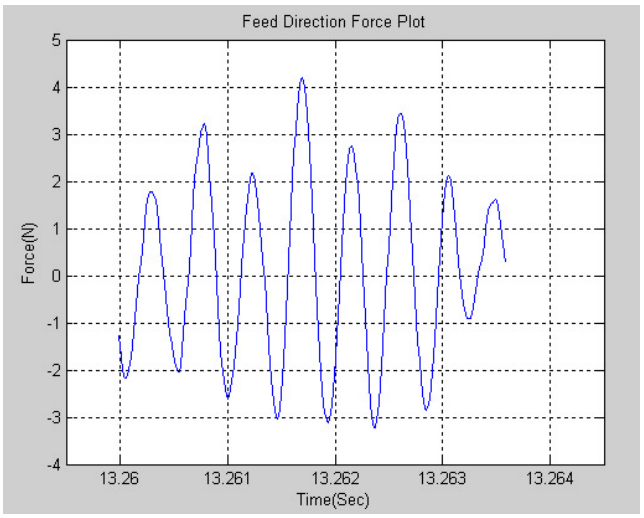

Figure 12. Cutting Force Plot for a 127µm Micro-Tool Cutting Aluminum

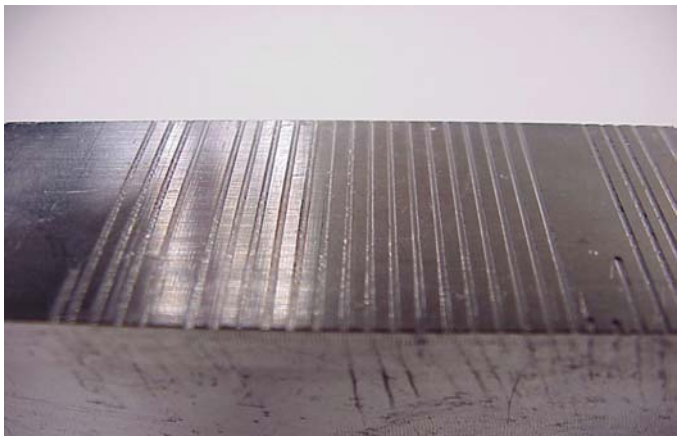

Figure 13. Cutting Test Slots in Aluminum Produced with a 508µm Tool

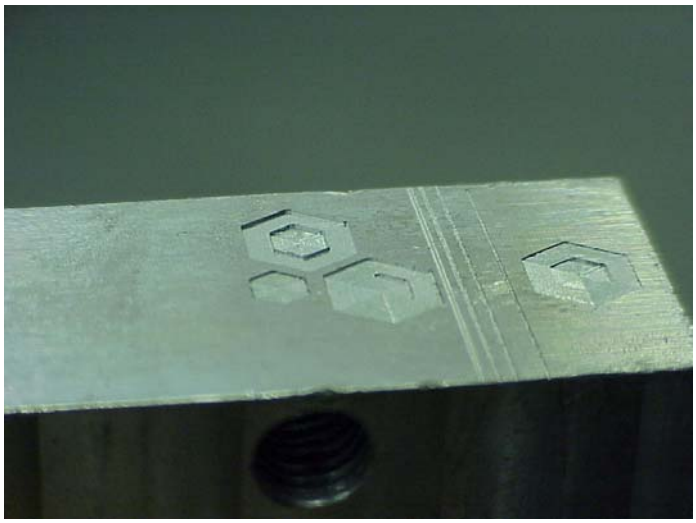

Figure 14. Hexagonal Cutting Test in Aluminum to Determine the Miniumum Wall Thickness Possible with a 254µm Tool

Summary of Spindle Generation 1 Testing

The testing of the spindle highlighted several problems with the first spindle design.

1. The combination of widely varying tool diameters and circularity along with the very small support area of the air bearing caused the tool shaft to strike the bearing at speeds in excess of 200,000 rpm. When this occurred, the air bearing became worn, and the ML-6 friction material was heated to the point that it melted.
2. Excessive runout in the tool tip showed that the bearing supporting the tool shaft needed to be stiffer, that the friction coating needed to be more compliant, that the friction wheel needed to be better balanced, and that the friction coating needed to be of more uniform thickness.
3. The excessive slip between the friction wheel and tool shaft showed the need for either a higher friction material, or the need for an intermediate diameter idler to produce better power transmission.

Testing performed on the first generation spindle to determine the operating envelope (at speeds up to 450,000 rpm) led to premature wear of the air bearing. Inspection of used tools revealed that carbon was deposited on the tool shaft during spindle rotation. The tool deposits tended to increase with operation time and rotation speed. Eventually, the air bearing bushing became measurably conical. To continue spindle evaluation, the porous carbon bearing was refurbished to original specifications by the manufacturer. However, operational tests of the refurbished prototype spindle were disappointing. The refurbished air bearing spindle appeared to be less capable then the original. Spindle operation experienced excessive runout and extraordinarily high wear rate of the porous carbon air bearing.

Regardless of the specific causes contributing to lackluster performance, previous concerns are confirmed. Runout, reduced maximum operating speed and wear rates associated with the refurbished first generation spindle are consistent with the suggested tasks drawn from the performance of the original spindle.

Ultra High Speed Spindle Design – Generation 2

Because of the challenges experienced with the first generation UHS spindle design, several significant modifications were made and a second generation spindle was created. This second spindle, shown in Figure 15, was created with the primary goals of addressing the issues raised in the analysis of the first generation spindle, notably the area and stiffness of the air bearing, the runout of the entire system, and issues specific to the friction wheel.

The drive wheel was redesigned in an attempt to reduce drive wheel runout. In contrast to the original design in which the drive wheel was a separate component mounted on a drive arbor, the second design utilized a drive wheel that was integral to the drive spindle arbor as shown in Figure 16. By combining these previously separate parts, mating alignment is eliminated. Reductions in drive wheel runout were predicted by simply changing to a single-piece aluminum design, providing inherently better alignment, balance and higher natural frequency. The monolithic drive spindle arbor and drive wheel was fabricated using processes comparable to the original drive wheel. Additionally, the ML-6 friction coating was replaced with a precision o-ring groove and an o-ring. The ML-6 had proven to be unevenly coated on the first generation

friction wheel and also exhibited too high a durometer, causing runout from the drive spindle to be transmitted to the tool shaft. O-ring materials (e.g., Buna-Nitrile and Polyurethane) were selected to provide a compliant drive interface and convenient replacement option.

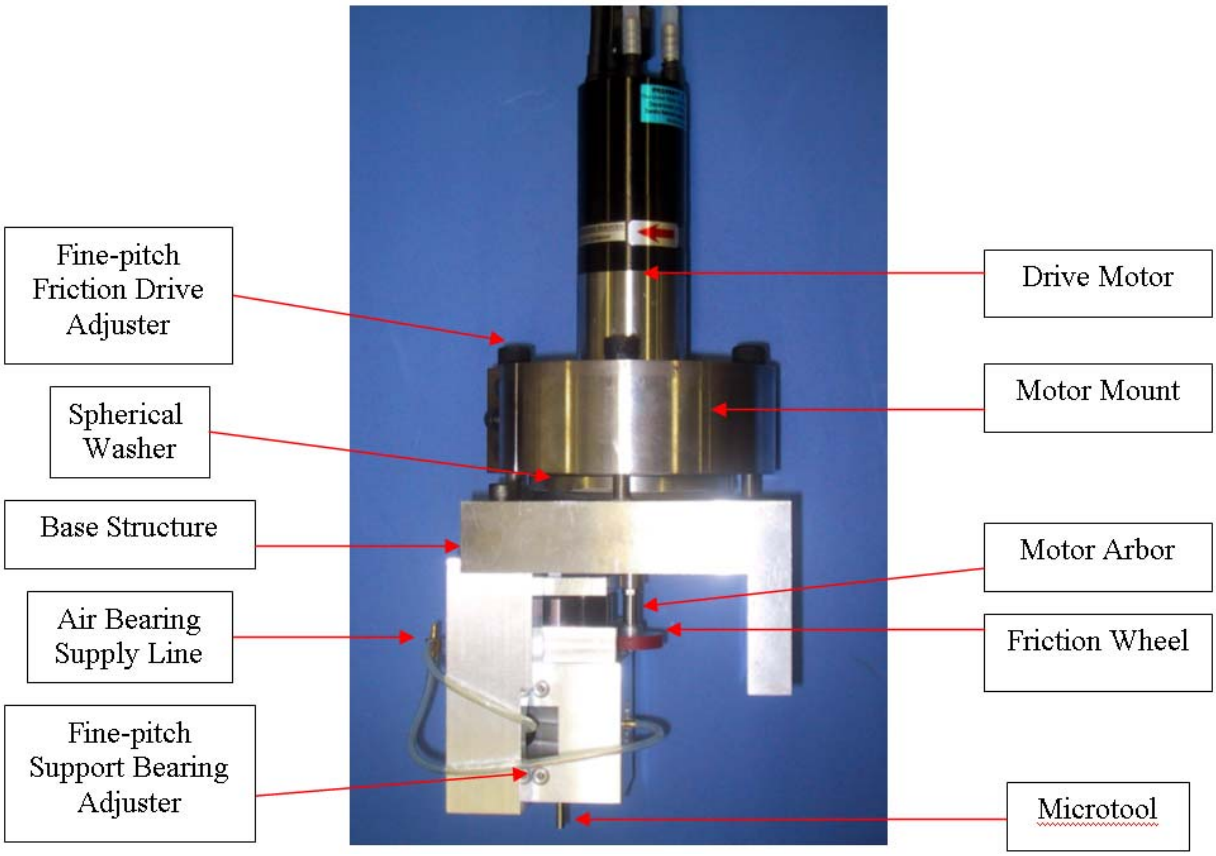

Figure 15. Ultra-High Speed Spindle - Design Generation 2

Figure 16. Integral and Two-Piece Friction Wheels Showing Different Friction Materials

Runout at the tool tip is dependent on spindle stiffness resulting from air bearing stiffness. Increases in radial stiffness and load support resulted from simply increasing the air bearing's dimensions. However, to increase air bearing bushing dimensions without increasing tool diameter, a novel rolling element design was created, departing from the previous design. Instead of supporting the tool directly in an air bearing spindle, the tool is supported on three equally spaced roller shafts that are in turn supported in air bearings of larger diameter as shown in Figure 17.

The Precise SC 40 Spindle is again used as the drive motor, mounted with the existing housing and bracket of the base structure. The single air bearing is replaced with a more complex assembly. The assembly has 3 overlapping bores in a triangular geometry. The bores each contain a partial air bearing housing that provides radial support to 3 precision ground carbide support roller shafts. These three support rollers each contact the tool shaft providing radial support along a portion of the tool shaft's length. The support rollers are positioned in the thrust direction by a flat air bearing on the drive end and by rare-earth magnets on the tool-tip end. The bearing housing contains fine thread pitch screws to provide accurate adjustment of the air bearings.

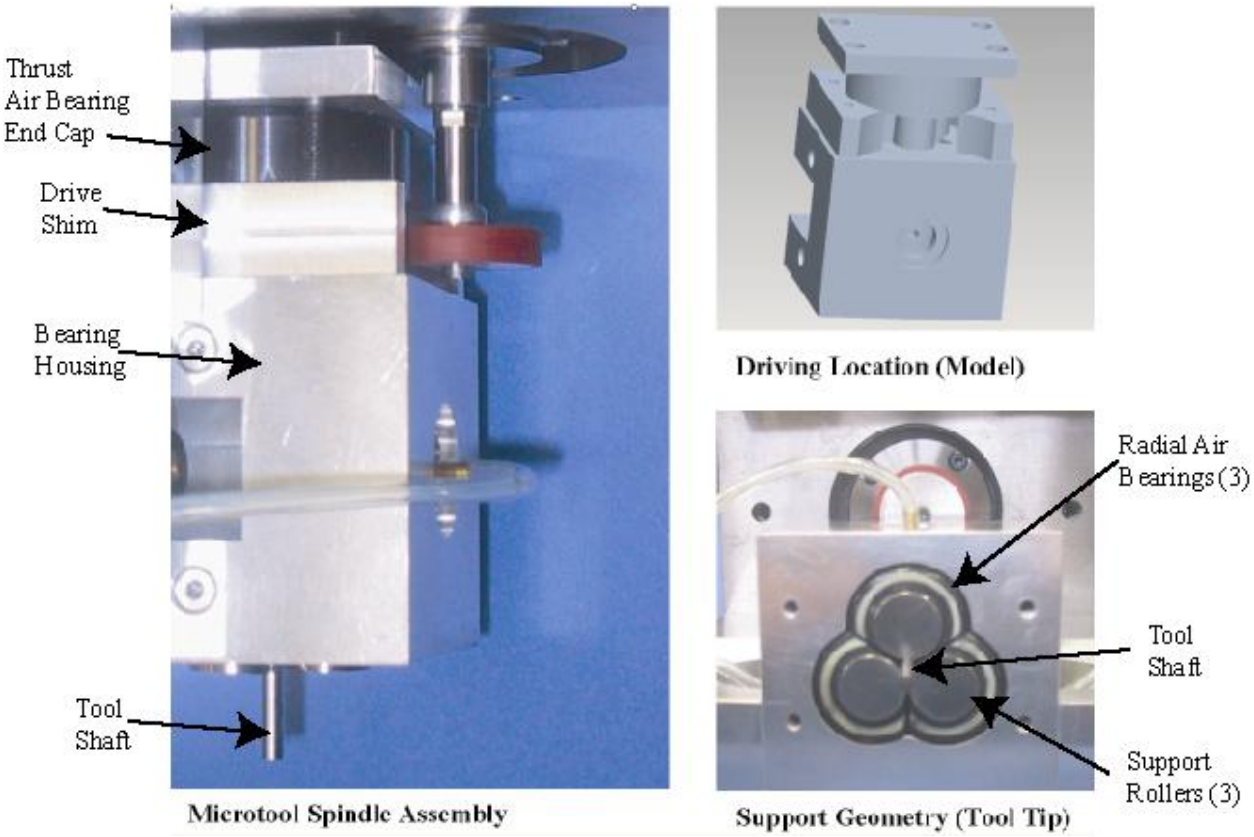

Figure 17. Rolling Element Bearing Assembly - Generation 2

The view of the solid model in Figure 17 shows the clearance region for the drive wheel. The drive shim provides access to the support roller that participates in the friction drive. The

thickness of the drive shim maintains sufficient clearance in the axial direction between the flat air bearing and bearing block.

The view taken along the axis of the tool shows the orientation of the support rollers about the tool. These support shafts, with diameters significantly larger than that of the tool shank, are supported in air bearings. This rolling element air bearing design allows for significant increases in bearing diameter while supporting the originally sized tool shank. This increase in bearing diameter increases bearing area and consequently increases load support and stiffness.

Air bearing radial load support and stiffness increase with bearing diameter and length. The spindle was redesigned with larger, 0.5 inch, partial air bearings. Length was also increased. Three shafts support the tool along 2 inches of its length. These shafts are equally spaced around the tool, one driven and two idlers.

The partial bushing air bearings were constructed from New Way Machine Components Inc. standard bushings (Part: S301201). The bearings were modified, at the University of Florida Machine Tool Research Center. The specialized fixture designed for manufacturing the partial bushings is shown in Figure 18 with a standard bushing mounted in the fixture ready for modification. The bearings are composed of an aluminum case and porous carbon bushing. The air bearing supply passages are grooves in the carbon and are oriented circumferentially along the aluminum bushing housing. A slot milling operation along the length of the bushing was necessary to relieve hoop stress apparently resulting from pressing the carbon stock into the aluminum shells. A slitting saw was then used to produce the final shape of the partial bushing as shown on the right side of Figure 18. Air passages, opened during machining along the length of the bushing, were sealed with epoxy to complete the manufacturing process.

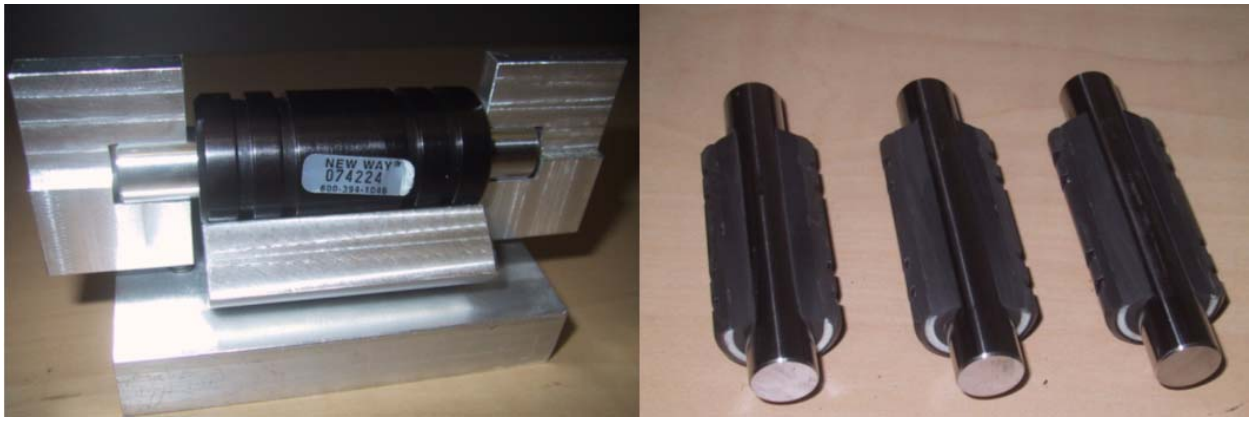

Figure 18. Fixture for Modifying Air Bearings (left) and Finished Partial Air Bearings with Shafts

Axial constraint of support shafts was implemented by a 1.5 inch flat air bearing (Part S104002). The opposing axial constraint was provided in two configurations. Permanent magnets recessed in the flat air bearing attracted the support shafts to preload the flat air bearing. In the case of insufficient constraint, opposing magnets on the ends of the shafts and spindle cap provided additional axial constraint through magnetic repulsive force.

Axial constraint of the microtool was similar to the first prototype spindle. Slightly inclined support shafts produced axial force that acted as preload against the thrust bearing. The porous carbon of the flat air bearing was used and provisions for a Teflon tool-contact surface were made.

Full assembly of the spindle, including alignment of the partial bushings, was completed at Sandia National Laboratories. Alignment of the support rollers was implemented using fine-pitch set screws. The set screws positioned the bushings. However, the alignment was not nearly as straightforward as expected. The manufacture of the partial bushing air bearings reduced the rigidity of the aluminum casings as they were no longer complete shells. Positioning the bushings with point load supports deformed the bushings slightly. This behavior changed the axis of the bushing and complicated the alignment of the support shafts.

Testing and Analysis of Generation 2 Spindle

Measurements of the revised drive wheel runout were made with the Lion Precision Spindle Error Analyzer (SEA) system. These measurements, shown in Figure 19, indicate that drive wheel runout was greater for the redesigned part. Although using an aluminum drive wheel arbor increases the natural frequency, it may also increase deflection as a result of the lower material modulus.

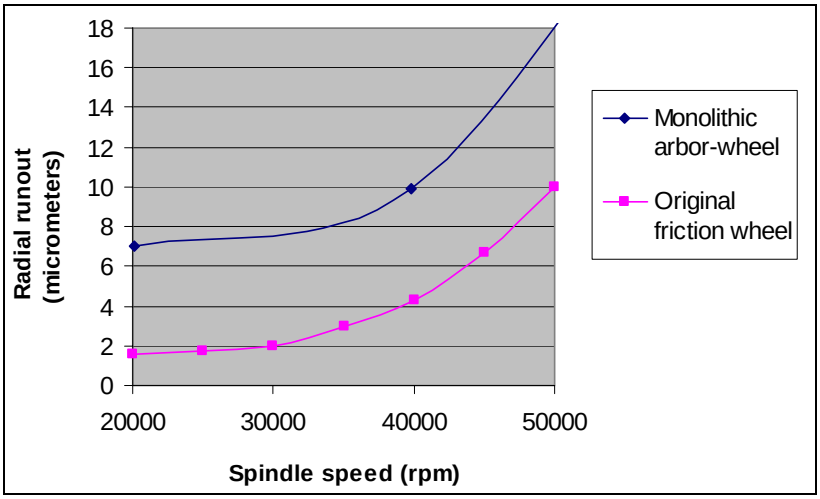

Figure 19. Total Indicated Runout of Drive Wheel Arbor on Generation 2 Spindle

It should be noted that the spindle speed is not measurable in the current SEA configuration, although FFT of the measurement data accurately implies the correct spindle speed. The zero-crossing algorithm used by the analyzer to determine spindle speed and radial error motions from a displacement signal is susceptible whenever asynchronous motions are dominant. A tachometer input is required to distinguish synchronous motions. However, measurements of Total Indicated Runout are not derived from angular position of the spindle and are considered accurate.

The materials tested for the drive wheel interface were also fairly viscoelastic. The viscoelastic properties of the materials produced excessive damping. The energy dissipated at the drive interface resulted in parasitic drive torque that severely limited operating speed.

Selection of drive wheel material reverted to the higher stiffness ML6 because it is less viscoelastic and demonstrated lower parasitic torque and power losses. Additionally, the dressed surfaces of the o-ring materials did not wear well at the speeds and contact loads required.

Operating the spindle generates excessive noise. Fast Fourier Transform (FFT) signal analysis of tool runout measurements clearly showed that frequency content was dominated by the drive spindle frequency and its first harmonic. This implied that runout from the drive spindle and drive wheel was being transmitted through to the tool.

Attempting to reduce transmitted runout, the drive wheel was single-point turned with a CBN (cubic boron nitride) tool to remove surface imperfections. Yet, drive spindle synchronous frequency content did not noticeably change.

The intensity of the harmonic at twice per revolution of the drive wheel implied that the drive wheel was out of round or on a skewed axis. Having already addressed the first implication, drive wheel skew was suspected. Skew induced runout is proportional to drive wheel thickness for flat face profile because a cylinder rotating on an axis that passes through its center, not coincident with its own, produces runout proportional to skew angle and cylinder thickness. A profile was machined into the drive wheel surface exhibiting a 1 degree relief angle to provide necessary clearance outside of the centerline contact.

These drive wheel modifications, however, did not noticeably reduce spindle noise. It is currently believed that this noise is generated by intermittent contact between the tool and support shafts. White light interferometry measurements of the worn tool and support shafts do not, as of yet, confirm this suspicion.

The operating envelope for spindle speed is not significant as the tool was not within desired runout limits. However, drive spindle speeds of above 30,000 rpm were tested (drive slip unknown).

The benefits associated with non-contact air bearings are conceded upon injecting a rolling contact into the tool supporting structure. Similar materials are often inadvisable for surfaces in contact and precision critical shafts should be spared repetitive surface interactions like those experienced by a high speed support roller. However, the nonlinear behavior of intermittent contact between support rollers and tool was the most negative result of the support roller design. The precision shafts acquired for use in the spindle were, in fact, not of sufficient cylindricity and roundness to give the desired smooth characteristics necessary for this application. The irregularities in the shafts produced excessive runout in the tool.

The friction drive posed additional challenges for spindle operation. The contact force between the friction wheel and support roller was provided by aligning the spindle drive and microtool spindle assembly. This was actuated by fine-pitch set screws that rotated the spindle with a

spherical washer. Contact forces were not easily adjustable and rarely repeatable. Additionally, the spherical washer was damaged over the course of the project and produced greater irregularity. Instead of specifying the drive wheel position that produces a drive wheel contact load, a force should be directly specified and applied for a more repeatable and adjustable contact load.

The need to accurately measure the characteristics of the spindle was not sufficiently addressed. Measuring tool error motions during high speed operation continues to challenge current capabilities.

Summary and Conclusions

This research effort produced 2 viable spindle designs for ultra-high speed milling of mesoscale features. The spindles were capable of speeds up to 450,000 rpm and performed milling tests at lower speeds. The research produced the following achievements:

- Two spindle designs were completed and tested. Finite element analysis was used to assure safety in the designs at speeds as high as 700,000 rpm.
- Previous literature was surveyed and an analysis of the most important spindle parameters was developed.
- Spindle Generation 1 achieved low runout and high speeds, though imbalance in the drivewheel caused runout to increase as the speed increased.
- Operational tool speeds of 450,000 rpm were achieved which is 250,000 rpm above currently available spindles. However, run time at these speeds was limited due to high wear rates in the spindle bearing.
- A computer interface to control the spindle while monitoring cutting forces and spindle parameters was completed and utilized.
- The friction drive system was shown to be capable of achieving ultra high speeds, but more investigation into friction interface materials is needed. The final material needs to be very uniform around the friction wheel, have a low enough durometer to isolate the tool shaft from drive spindle error and collet mounting error.
- Rotational error in the spindle generation 1 drive system caused runout in the spindle while insufficient support of the tool caused high bearing wear rates. The second generation spindle suffered from difficulty in the alignment and utilization of the 3 roller support bearings. These problems caused higher drive forces and the limited torque of the drive spindle prevented the system from achieving ultra high speeds. Additionally, the support bearings were not as cylindrical as expected leading to more tool runout.

The initial concept is still very good and should be pursued. The following are issues that were identified in this project that should be considered in future efforts.

- The drive wheel needs to have more precision in its initial manufacture to assure the highest degree of balance is achieved. These items should be diamond turned while mounted in the spindle of the electric drive spindle.
- It is worth investigating alternative, non-contact drive methods due to the failure of the friction interface. Possibilities include air turbine drives or even magnetic drives of

some type. Careful consideration should be given to whether a solution can be added to a stock tool, rather than requiring very expensive custom tools.

- The utilization of stock tools may not be possible due to tool runout and geometry. Very few tool manufacturers thought that they could make a tool with the desired runout and concentricity requirements
- Larger tool shafts might be necessary to increase the support in the air bearing, though this also increases the inertia of the tool and the stresses when running at extremely high speeds.

References

1. W. Y. Bao, I. N. Tansel, “Modeling micro-end-milling operations, Part I: analytical cutting force model”, International Journal of Machine Tools & Manufacture 40(2000) 2155-2173.
2. J. Tlusty, P. Macneil, “Dynamics of cutting forces in end milling”, Annals of the CIRP 24(1)(1975) 21-25.
3. W. Y. Bao, I. N. Tansel, “Modeling micro-end-milling operations, Part II: tool ru-out”, International Journal of Machine Tools & Manufacture 40(2000) 2175-2192.
4. Kiha Lee, Sung-Hoon Ahn, David A. Dornfeld and Paul K. Wright, “The effect of run-out on design for manufacturing in micro-machining process”.
5. Michael P. Vogler, Richard E. DeVor, Shiv G. Kapoor, “Microstructure-level force prediction model for micro-milling of multi-phase materials”.
6. M. Rahman, A Senthil Kumar, J.R.S. Prakash, “Micro-milling of pure copper”, Journal of Materials Processing Technology 116(2001) 39-43.
7. W. Y. Bao, I. N. Tansel, “Modeling micro-end-milling operations, Part III: influence of tool wear”, International Journal of Machine Tools & Manufacture 40(2000) 2193-2211.
8. I. N. Tansel, T. T. Arkan, W. Y. Bao, N. Mahendrakar, B. Shisler, D. Smith and M. McCool, **“**Tool wear estimation in micro-machining, Part I: tool usage–cutting force relationship”, International Journal of Machine Tools & Manufacture 40(2000) 599-608.
9. Craig R. Friedrich and Michael J. Vasile, “Development of the micro milling process for high aspect ratio microstructures”, Journal of Microelectromechanical Sytems, Vol. 5, No.1, March 1996.
10. Arthur P. Boresi, “Advanced Mechanics of Materials”.
11. Jiri Tlusty, “Manufacturing Processes and Equipment”.

Distribution

Qty.	Mail Stop	Name	Organization
1	MS 0123	LDRD Donna Chavez	01011
2	MS 0899	Technical Library	09616
4	MS 0958	David Gill	14132
1	MS 0958	Gilbert Benavides	14132
1	MS 1310	Bernhard Jokiel Jr.	01745
1	MS 9018	Central Technical Files	8945-1
2	External Mailing	Dr. John Ziegert & Scott Payne University of Florida Mechanical & Aerospace Receiving Room No. 002, Bldg. 183 Gainesville, FL 32611	